

---

**Arařtırma Makalesi / Research Article**

---

**A Numerical Study on the Large Displacement in Functionally Graded Beam under Thermal Effect**

Ersin DEMİR

Pamukkale University, Faculty of Technology, Department of Mechatronics Engineering, Denizli, Turkey,  
ORCID ID: <https://orcid.org/0000-0001-8222-5358>, edemir@pau.edu.tr

**Geliř/ Received:** 21.09.2023;

**Kabul / Accepted:** 02.11.2023

**ABSTRACT:** The large displacement behavior of a Functionally Graded (FG) beam under uniform thermal load is investigated numerically. Six different effects are taken into consideration when examining the large displacement behavior of the beam. These are the effects of temperature, material, geometry, slenderness, force, and boundary conditions. The nonlinear numerical analysis is carried out by using the Simulation mode of SolidWorks, which is a finite element-based commercial program. It is obtained from the results that the displacement of the end of the beam increases with increasing temperature, slenderness ratio, and force. It is also found that it decreases with increase in the ratio of ceramic in Functionally Graded Material (FGM). Moreover, the displacement of the end of the beam decreases with increasing the width of the beam. Furthermore, as expected, the maximum and minimum displacements are obtained in the beams with Clamped-Free and Clamped-Clamped boundary conditions, respectively.

**Keywords:** Large displacement, Beam, FGM, Thermal load

---

\*Sorumlu yazar / Corresponding author: edemir@pau.edu.tr

Bu makaleye atıf yapmak için /To cite this article

Demir, E. (2023). A Numerical Study on the Large Displacement in Functionally Graded Beam under Thermal Effect. Journal of Materials and Mechatronics: A (JournalMM), 4(2), 492-503.

## 1. INTRODUCTION

Some structural elements can be exposed to large displacement without exceeding their yield stress. Therefore, the large displacement problem in a structural element, especially in a beam, under force effect has attracted the attention of many researchers. Many studies have been done on this subject in the last decade. Some of these studies published in recent years are mentioned below. Khosravi and Jani (2018) proposed two novel numerical techniques to solve large displacements of cantilever beams with mixed boundary conditions. They compared their proposed mathematical model results with the results obtained from the experiment. Li and Li (2019) considered the three-point bending study of a Timoshenko beam. They analyzed the large displacement and rotation of the beam. Moreover, they compared calculated results with experimental data. Tari et al. (2015), overcame the large displacement problems of Euler-Bernoulli cantilever beams under a force and moment. They presented the solutions for different loading in cartesian coordinates. Furthermore, they developed piecewise parametric large displacement solutions. Kimiaefar et al. (2014), overcame a solution of the large displacement of a cantilever beam. They used the Homotopy Analysis Method (HAM) in their analysis. Mohyeddin and Fereidoon (2014) examined the large displacements of a shear-deformable beam under a point load. They obtained an equation system based on Timoshenko's theory. Kimiaefar et al. (2012) studied the large displacement of a Euler-Bernoulli beam which has variable flexural rigidity. They solved the problem by HAM. They found the characteristics of the displacement of a beam under a follower force. Kimiaefar et al. (2011) studied the large displacement and rotation of a beam subjected to static loading. They solved the governing equation of this problem by HAM. They compared their results with the results obtained from the Range Kutta method. Chen (2010) proposed an approach to solve the large displacement of a cantilever beam.

Although there have been many studies on composites (Ünal et al., 2022) or FGMs (Demir et al., 2022) in recent years, there are relatively few studies on the large displacement of beams made by FGM in the literature. Some of them, encountered in the open literature, are given below. Zhou et al. (2018) presented a study on the large deflection of a FG beam subjected to transverse loading. They obtained a yield criterion for a FG beam. They formulated analytical solutions for the large displacements of beams using proposed criteria and compared their solution with numerical solutions. Horibe and Mori (2018) investigated a bending problem for axially FG tapered beam under transverse load by using the Runge-Kutta method. Using a finite element method, Gan and Kien (2014) overcame the large displacement behavior of FG beams resting on an elastic foundation. They used a method that combined the arc-length control method with the incremental iterative method. Sitar et al. (2014) solved the equation of large displacements of a non-homogeneous beam. They solved equations numerically and tested on some examples. Mien and Gan (2014) analyzed the large displacements of tapered FG beams. They solved the large displacement problem by using the arc-length control algorithm. Davoodinik and Rahimi (2011) studied the bending problem of a tapered FG beam under inclined end and intermediate loadings. They introduced a curvilinear coordinate system to obtain the governing equations for large deformation. They used semi-analytical methods in their study and compared their results with the existing solution. Kang and Li (2010) investigated the large deformation of a FG beam. They obtained an expression for rotation and displacement in a FG beam under the end moment. They investigated the effects of variations in the Elasticity modulus and the material property on the bending of the FG beam. Rahimi and Davoodinik (2010) studied the large displacement behavior of a FG beam under inclined end loading by using the analytical and Adomian Decomposition Method (ADM). They also used a solver based on finite element analysis to solve the equation. They showed that the ADM is useful in solving such problems.

As the literature is surveyed, it can be seen that the problem of large displacement of beam subjected to the thermal effect, is quite limited. Li and Song (2006) determined the non-linear deformation of beams under mechanical and thermal loads. They solved the equation by using the Shooting Method. They analyzed the thermal large displacements of Timoshenko beams with fixed-fixed and pinned-pinned ends. Yin and Wang (2004) obtained the results of the large displacement of the beam under temperature loads numerically. He investigated the effect of different temperature distributions, loads, and stiffness on displacement.

In the study, the large displacement behavior of FG beam with variable cross-section under uniform thermal load is studied numerically. The effects of the temperature, material, geometry, slenderness, force, and boundary condition on the displacement of the end FG beam are investigated. From the open literature research, no similar study could be found.

## 2. MODEL

In Figure 1, a FG beam with variable cross-section is shown. The dimensions of the beam are given as follows: The width at the clamped end ( $b_o$ ) is 20 mm, while the width at the free end ( $b_L$ ) is 5 mm.  $h$  is the thickness and equal to 1 mm and  $L$  is the length of the beam and equal to 200 mm. Moreover,  $F$  is transverse force and is equal to 5N.

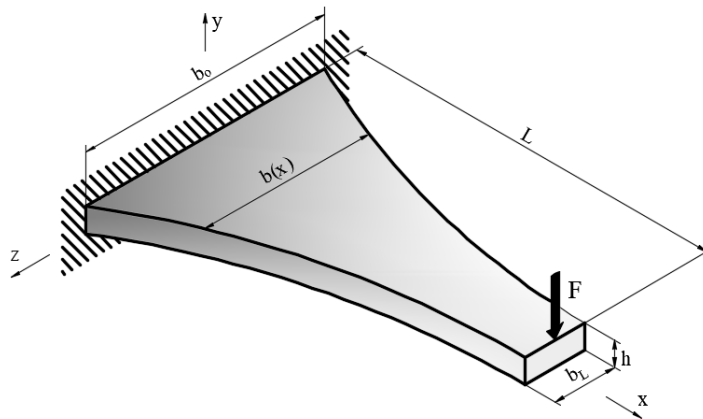


**Figure 1.** FG beam with variable cross-section

As can be seen from the figure, the beam exhibits varying width along its length and the width is given by the formula below.

$$b(x) = (b_L - b_o) \left(\frac{x}{L}\right)^k + b_o \quad (1)$$

In Equation 1,  $x$  is the distance from the clamped end along the  $x$  direction and  $k$  is geometric index. When  $k$  is equal to zero, the beam's width is equal to 5 mm and constant. When  $k$  approaches infinity, the width of the beam is also constant and equal to 20 mm. The  $k$  is taken as 0.5, 1, and 2. The variation of beam width by geometric index is represented in Figure 2. From the figure, it can be observed that the width of the beam decreases linearly when  $k$  is equal to 1. However, when  $k$  is equal to 0.5 and 2, the decrease in beam width is curved and these curves are convex and concave, respectively.

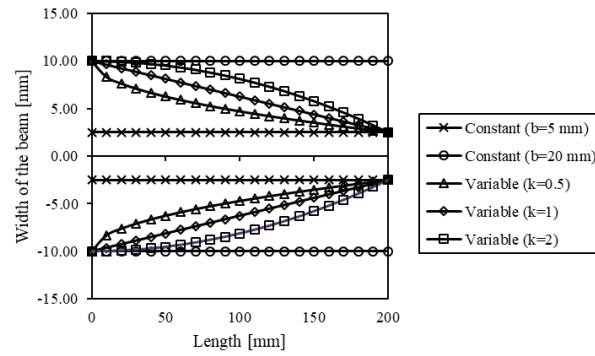


**Figure 2.** Variation of beam width by geometric index

### 3. MATERIAL

The beam is made of FGMs, which is obtained by volumetric mixing of Stainless Steel (SUS304) and Aluminum Oxide ( $\text{Al}_2\text{O}_3$ ). As known, the material properties vary with change in the temperature. Shen (2009) gave the following equation. This equation gives the temperature-dependent material properties.

$$P_j = P_0(P_{-1}T^{-1} + 1 + P_1T + P_2T^2 + P_3T^3) \quad (2)$$

where  $T$  is the temperature in Kelvin ( $K$ ) and  $P_i$  ( $i = -1, 0, 1, 2, 3$ ) is the coefficient listed in Table 1.  $P_j$  is material properties.  $E$  is the elasticity modulus in Pascal ( $Pa$ ),  $\nu$  is Poisson's ratio,  $\alpha$  is the thermal expansion coefficient per Kelvin ( $K^{-1}$ ), and  $\kappa$  is thermal conductivity in Watts per meter Kelvin ( $W/mK$ ) of the steel and ceramic.

**Table 1.** Coefficients of material properties (Shen, 2009)

	$E [Pa]$		$\nu$		$\alpha [K^{-1}]$		$\kappa [W/mK]$	
	SUS304	$\text{Al}_2\text{O}_3$	SUS304	$\text{Al}_2\text{O}_3$	SUS304	$\text{Al}_2\text{O}_3$	SUS304	$\text{Al}_2\text{O}_3$
$P_0$	201.04e+9	349.55e+9	0.3262	0.2600	12.330e-6	6.8269e-6	15.379	-14.087
$P_{-1}$	0	0	0	0	0	0	0	-1123.6
$P_1$	3.079e-4	-3.853e-4	-2.002e-4	0	8.086e-4	1.838e-4	-1.264e-3	-6.227e-3
$P_2$	-6.534e-7	4.027e-7	3.797e-7	0	0	0	2.092e-6	0
$P_3$	0	-1.673e-10	0	0	0	0	-7.223e-10	0

To see the temperature effect, the temperature of the beam is increased from 22 °C to 400 °C. The temperature is increased by interval of 100 °C between 100 °C and 400 °C. The material properties of steel and ceramic are calculated from Equation 2 and Table 1 for each temperature. The densities of the steel and ceramic are assumed as constant due to the minor change in temperature increase. The densities of the steel and ceramic are taken as 8166  $\text{kg/m}^3$  and 3750  $\text{kg/m}^3$ , respectively (Shen, 2009).

The material characteristics of the FG beam vary from one end to the other. The following equation is used to determine the material properties of the beam in the study,

$$MP = (MP_s - MP_c) \left(\frac{x}{L}\right)^n + MP_c \quad (3)$$

where  $MP$  is the material properties of the whole beam.  $MP_s$  and  $MP_c$  are material properties of steel and ceramic, respectively. As abovementioned, the material properties are  $E$ ,  $\nu$ ,  $\alpha$ , or  $\kappa$ .  $x$  is the distance along the length from one end of the beam and  $n$  is material index. This equation is similar to the equation given (Shen, 2009). According to Equation 3, the effects of the variations in the  $T$

[°C] and  $n$  on the abovementioned material properties along the beam length are shown as follows, respectively.

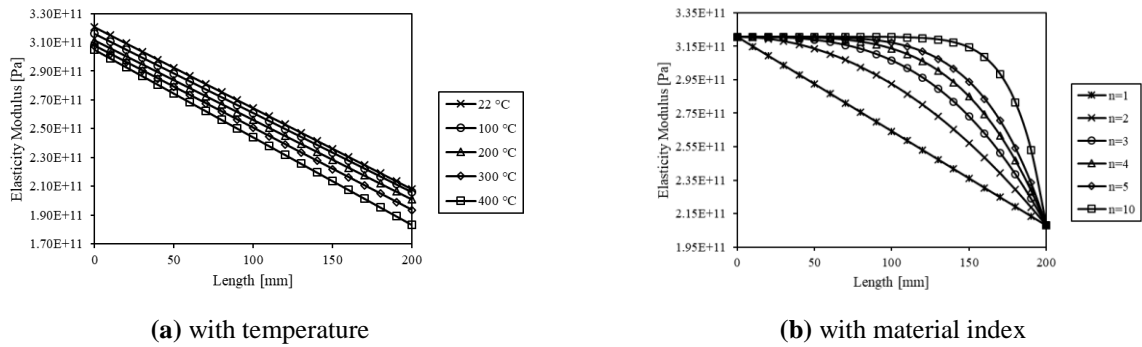


**Figure 3.** Variation in elasticity modulus

Figures 3(a) and (b) depict the changes in the elasticity modulus along the beam's length with respect to temperature and material index  $n$ , respectively. It can be seen from the above two figures that the beam's leftmost end is Stainless Steel and the rightmost end is Aluminum Oxide. It is seen in Figure 3(a) that the Elasticity Modulus decreases gradually with increasing temperature. However as depicted in Figure 3(b), the elasticity modulus exhibits a hyperbolic increase along the length of the beam as the material index rises.

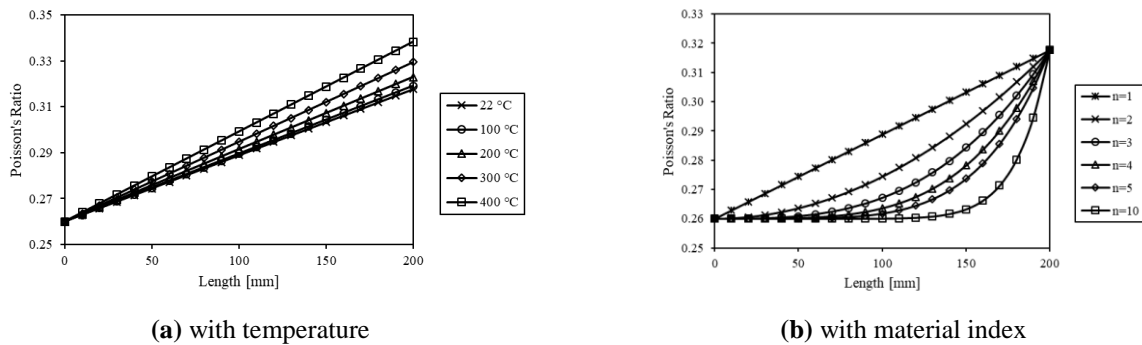


**Figure 4.** Variation in Poisson's ratio

The variation in Poisson's ratio is depicted in Figure 4. Figure 4(a) indicates that as the temperature increases, Poisson's ratio also increases. As depicted in Figure 4(a), the increase in displacement is greater at the free end of the beam in comparison to the clamped end. Moreover, the difference at the free end is quite low at low temperatures. Figure 4(b) shows the Poisson's ratio decreases throughout the beam's span with increasing the material index  $n$ .

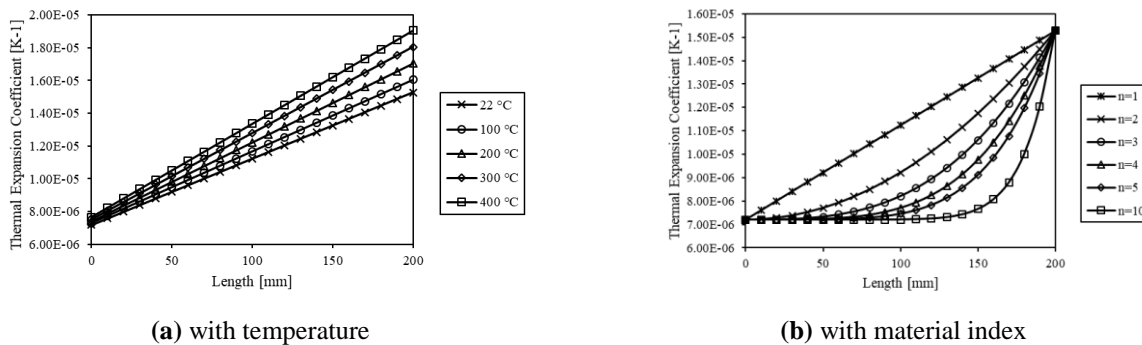


**Figure 5.** Variation in the thermal expansion coefficient

The change in the coefficient of thermal expansion is shown in Figure 5. It is seen from Figures 5(a) and 4(a) that the figure obtained for the thermal expansion coefficient is similar to the figure obtained for Poisson's ratio. But, contrary the Figure 4(a), the differences at the free end are almost the same here. Figure 5(b) represents the thermal expansion coefficient decreases across the longitudinal axis of the beam with increasing the material index  $n$ .

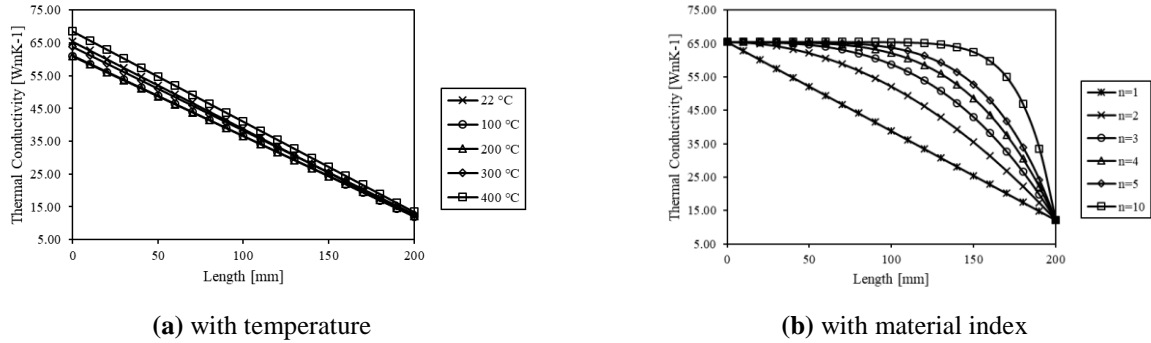


**Figure 6.** Variation in thermal conductivity

The thermal conductivity variation is shown in Figure 6. Unlike the coefficient of thermal expansion, the thermal conductivity decreases with increasing temperature, as seen in Fig 6(a). Figure 6(b) shows the thermal conductivity increases over the entire length of the beam with increasing the material index  $n$ .

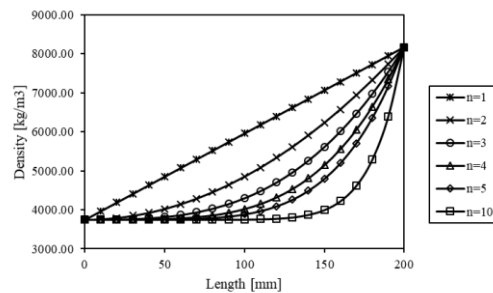


**Figure 7.** Variation in density with material index

In this study, it is assumed that the density does not change with temperature. Figure 7 shows the variation in density with material index  $n$ . As can be seen, the density decreases along the length of the beam with increasing  $n$  index.

#### 4. NUMERICAL SOLUTION

The numerical thermal large displacement behavior of the beam is overcome by the SolidWorks program. SolidWorks is a program that can perform both drawing and analysis of engineering structures. So, this program is used for both drawing and large displacement analysis. Firstly, the wireframe model of the beam is drawn. The program allows curve drawing with equation. Therefore, wireframe of a beam with variable width according to Equation 1 is drawn easily. The resulting wireframe model is then converted to a planer surface model. The beam material is defined separately as a special material given in Section 3. After the model is completed, the Simulation mode of the SolidWorks program is launched for the analysis. In the Simulation mode of the program, both thermal and static analyses are performed on the beam. Intel Direct Sparse is used as a solver in both analyses. The thickness of the beam is defined in the Simulation mode of the program. Moreover,

after thermal loads are defined, the beam is meshed and the thermal analysis is executed. The data obtained from thermal analysis are transferred to static analysis. Again, after the supports and loads are defined, the beam is meshed and the nonlinear static analysis is executed. The meshed model and the case after analysis of the beam with  $k=1$  are shown in Figures 8(a) and (b), respectively. The mean node number and the mean element number are obtained 2737 and 1260 respectively for the beam with  $k=1$  as a result of the meshed process. As a result of both analyses, large displacement values at the end of the beam are obtained.

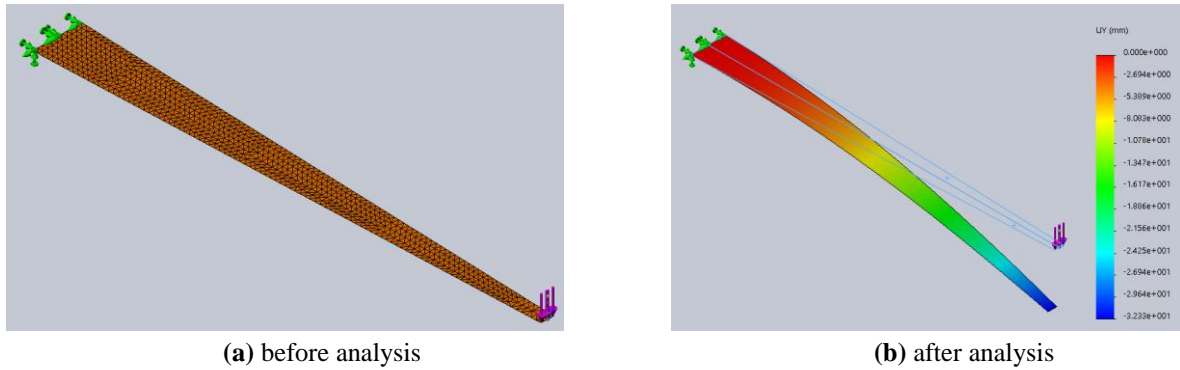


Figure 8. Simulation model of the variable beam

### 5. RESULTS AND DISCUSSION

The numerical thermal large displacement behavior of the FG beam with variable cross-section is done in the analysis. The effects of temperature, material, geometry, slenderness, force, and boundary conditions are examined in the following subsections, respectively.

#### 5.1 Effects of Temperature

Some assumptions are made only to see the temperature effect. The beam edge condition is taken as Clamped-Free (C-F). The beam's longitudinal, transverse, and thickness dimensions are taken as constant and they are 200 mm, 20 mm, and 1 mm, respectively. Since the material index  $n$  is taken 1, the beam material is FGM. The force is applied at the free end of the beam and the value of the force is taken 5 N. The temperature is raised in increments of 100°C, starting from 100°C and reaching 400°C. The room temperature (22 °C) is also taken into consideration in the analysis.

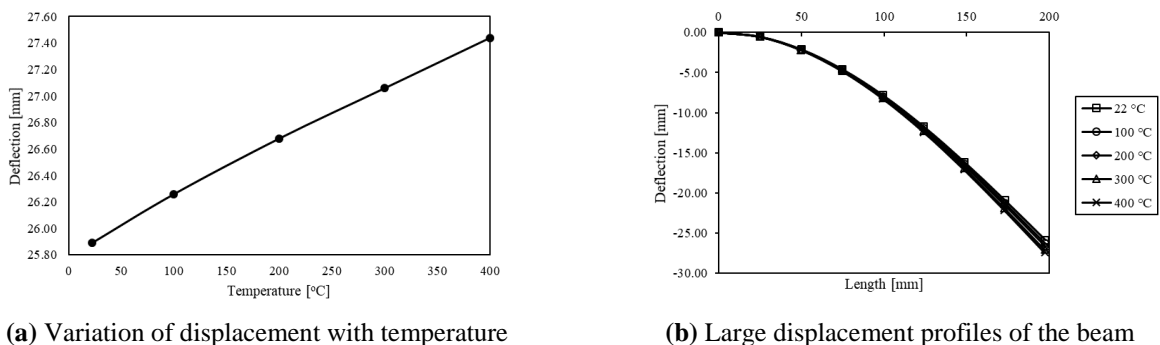


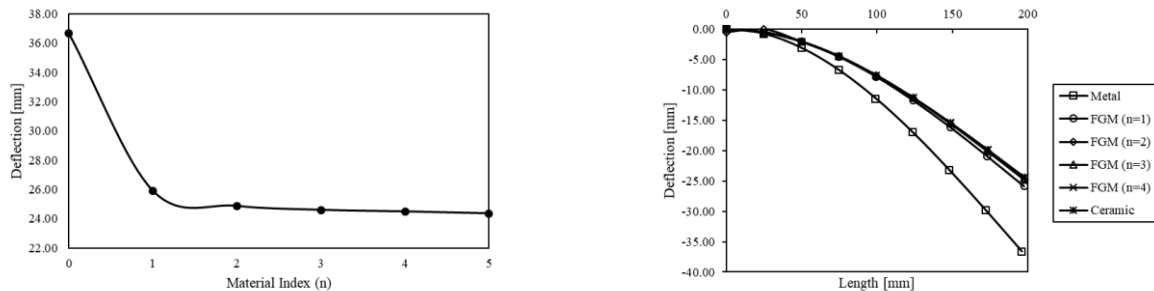
Figure 9. Effect of temperature

Figures 9(a) and (b) show the variations of the large displacement values at the beam's endpoint and the large displacement profiles of the beam with temperature, respectively. The figures show that the displacement of the free end of the beam rises with the rising temperature. As compared to the

displacement at 400 °C and 22 °C, there is a difference of about 1.5 mm. Therefore, it can be said that the increase in temperature does not affect the amount of displacement excessively.

### 5.2 Effects of Material Index ( $n$ )

To see the effect of the material, the material index is chosen between 0 and 4 by 1 increment. The material of the beam is pure steel according to Equation 3 when  $n=0$ . Pure ceramic material is also taken into account in the analysis. Increase in material index converts the beam material from steel to ceramic. So, when  $n$  is equal to infinity, the beam material is pure ceramic. The boundary condition of the beam is taken as C-F. The beam is assumed to have constant dimensions: a length of 200 mm, a width of 20 mm, and a thickness of 1 mm. The temperature is accepted 22 °C. The force value is chosen 5 N.



(a) Variation of displacement with  $n$

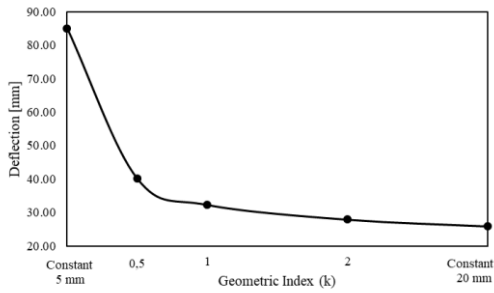
(b) Large displacement profiles of the beam

**Figure 10.** Effect of material index

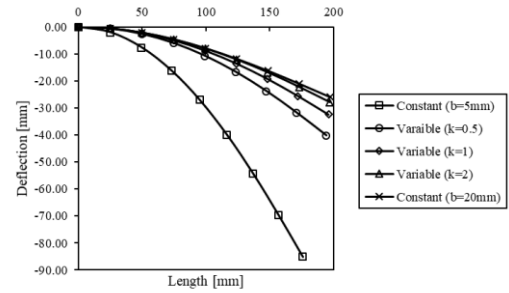
Figures 10(a) and (b) depicted the variations of the large displacement of the end of the beam and the large displacement profiles of the beam with material index, respectively. Figures 10(a) and (b) show that displacement at the free end of the steel beam is much greater than the FGM and ceramic beam. The difference appears to be approximately 10 mm. Furthermore, it is also seen from the figures that the displacement of the free end of the beam decreases with increasing the ratio of ceramic in FGM but, the decrease is quite low. Therefore, it can be said that the use of FGM significantly reduces displacement as compared with the use of steel.

### 5.3 Effects of Geometric Index ( $k$ )

To examine the effect of the geometry, the geometric index is taken as 0, 0.5, 1, and 2. The width of the beam is constant and equal to 5 mm according to Equation 1 when  $k=0$ . Increase in the geometric index changes the width of the beam from 5 mm to 20 mm. So, when  $k$  is equal to infinity, the width of the beam is equal to 20 mm. The boundary condition of the beam is taken C-F. The length and thickness of the beam are taken constant and 200 mm and 1 mm, respectively. The material index  $n$  is taken 1 so that the beam material is FGM. The temperature and the force are chosen 22 °C and 5 N, respectively.



(a) Variation of displacement with k



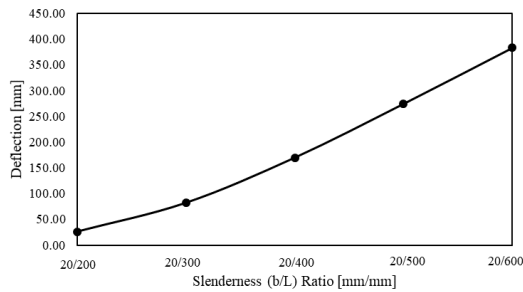
(b) Large displacement profiles of the beam

Figure 11. Effect of geometric index

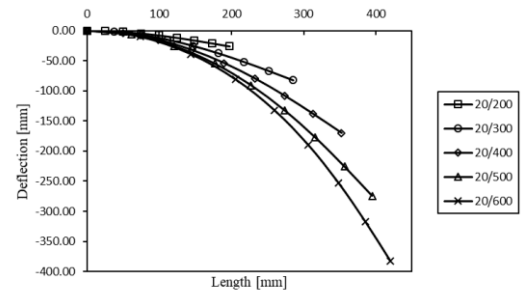
The variations of the large displacement at the free end of the beam and the large displacement profiles of the beam with geometric index are represented in Figures 11(a) and (b), respectively. The figures show that the displacement at the end of the beam decreases with increasing the geometric index. The figures clearly indicate a considerable variation between the beams having widths of 5 mm and 20 mm. The results show that the displacement in the convex-shaped tapered beam ( $k=0.5$ ) is more than that of the concave-shaped tapered beam ( $k=2$ ).

5.4 Effects of Slenderness Ratio

To see the effect of the slenderness ratio ( $b/L$ ), the width and the thickness of the beam are taken constant and equal to 20 mm and 1 mm, respectively. Meanwhile, the beam's length is incrementally raised from 200 mm to 600 mm, with increments of 100 mm. The boundary condition of the beam is taken C-F. The temperature, force, and material index  $n$  are again taken 22 °C, 5 N, and 1, respectively.



(a) Variation of displacement with slenderness ratio



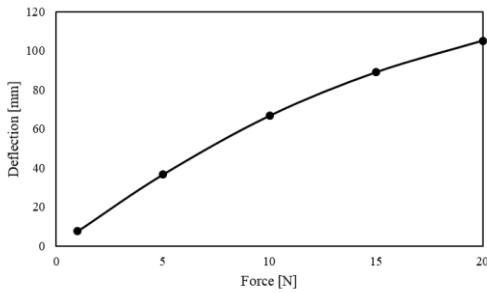
(b) Large displacement profiles of the beam

Figure 12. Effect of slenderness ratio

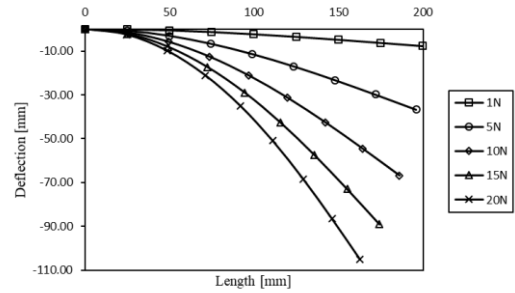
Figures 12(a) and (b) depict the variations of the large displacement at the free end of the beam and the large displacement profiles of the beam with slenderness ratio, respectively. It is seen from the figures that the displacement of the free end of the beam increases gradually with increasing slenderness ratio. According to the figures, the end-point displacement of the beam increases almost fifteen times when the length of the beam increases threefold.

5.5 Effects of Force

The material of the beam is chosen as pure steel to see the effect of force on the large displacement. Hence, the material index is equal to zero. The temperature is taken 22 °C. The width, thickness, and length of the beam are taken 20 mm, 1 mm, and 200 mm, respectively. The force is exerted on the free end of the beam. The force is increased from 1 N to 20 N. The beam is assumed to have a C-F boundary condition.



(a) Variation of displacement with force



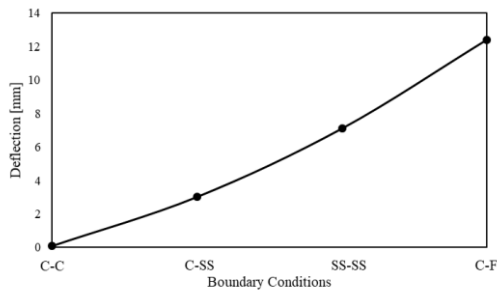
(b) Large displacement profiles of the beam

Figure 13. Effect of force

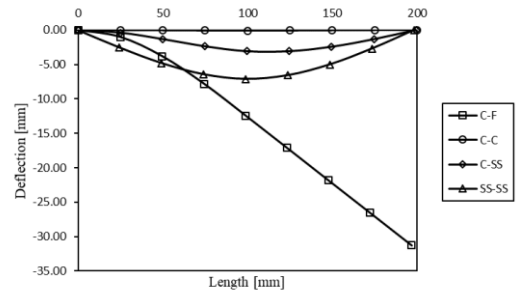
Figures 13(a) and (b) represent the variations of the large displacement at the free end of the beam and the large displacement profiles of the beam with forces, respectively. The figures show that the displacement increases with increasing force, as expected. According to the results, there is a direct proportional relationship between the applied force and the displacement at the beam's end.

### 5.6 Effects of Boundary Conditions

In order to see the effect of boundary conditions, four types of boundary conditions are taken into account. They are Clamped-Free (C-F) boundary condition, Clamped-Clamped (C-C) boundary condition, Clamped-Simply Supported (C-SS) boundary condition, and Simply Supported-Simply Supported (SS-SS) boundary condition. Since the material index  $n$  is taken 1, the beam material is FGM. The length, width, and thickness of the beam are taken constant and 200 mm, 20 mm, and 1 mm, respectively. The temperature is taken 22 °C. To ensure consistent comparisons among various boundary conditions, the force is exerted at the midpoint of the beam. Moreover, the force is chosen 20 N. This is because, when 5 N is applied to the beam with C-C boundary conditions, the displacement value is quite small.



(a) Variation of displacement with boundary conditions



(b) Large displacement profiles of the beam

Figure 14. Effect of boundary conditions

From Figures 14(a) and (b), one can observe the changes in large displacement at the midpoint of the beam and the corresponding large displacement profiles across various boundary conditions. It is seen from the figures that, the beam with C-F boundary condition exhibits the maximum displacement at its midpoint. It can be also seen from Figure 14(b) that the displacement after the midpoint of the beam with the C-F boundary condition is linear, not curvilinear, as expected. Because the force is applied at the midpoint of the beam. It can be seen from Figure 14(a) that displacement increases gradually as the boundary condition changes from C-C to C-F.

## 6. CONCLUSION

This study aims to examine the large displacement behavior of a FG beam with a variable cross-section subjected to uniform thermal loading. The following results are obtained from the study:

- The displacement at the free end of the beam under the force increases with increasing temperature. But this is relatively small.
- The addition of ceramic powder to the beam material significantly reduces the displacement at the free end of the beam. However, the increase in the volume fraction ratio of ceramic in FGM does not affect the displacement at the free end of the beam too much.
- The displacement at the end of the beam decreases with increasing the beam width. In addition, the displacement at the end of the convex-shaped tapered beam ( $k=0.5$ ) is more than that of the concave-shaped tapered beam ( $k=2$ ).
- The displacement at the beam's free end increases gradually with increasing slenderness ratio.
- The displacement at the end of the beam increases with increasing force.
- The minimum displacement in the midpoint of the beam is obtained in the beam with the C-C boundary condition.

## 7. CONFLICT OF INTEREST

Author approve that to the best of their knowledge, there is not any conflict of interest or common interest with an institution/organization or a person that may affect the review process of the paper.

## 8. AUTHOR CONTRIBUTION

The entire responsibility for the research lies with Ersin Demir, encompassing the acquisition of the theoretical framework through a review of relevant literature, conducting numerical analyses for data collection, ensuring the overall harmony of the text during the writing process, and making corrections and revisions.

## 9. REFERENCES

- Chen L., An integral approach for large deflection cantilever beams. *International Journal of Non-Linear Mechanics* 45(3), 301-305, 2010.
- Davoodinik A.R., Rahimi G.H., Large deflection of flexible tapered functionally graded beam. *Acta Mechanica Sinica* 27(5), 767-777, 2011.
- Demir E., Sayer M., Callioglu M., An approach for predicting longitudinal free vibration of axially functionally graded bar by artificial neural network. *Proceedings of the Institution of Mechanical Engineers, Part C: Journal of Mechanical Engineering Science* DOI: 10.1177/09544062221141246, 2022.
- Gan B.S., Kien N.D., Large Deflection Analysis of Functionally Graded Beams Resting on a Two-Parameter Elastic Foundation. *Journal of Asian Architecture and Building Engineering* 13(3), 649-656, 2014.
- Horibe T., Mori K., Large deflections of tapered cantilever beams made of axially functionally graded material. *Mechanical Engineering Journal* 5(1), DOI: 10.1299/mej.17-00268, 2018.

- Kang Y.A., Li X.F., Large Deflections of a Non-linear Cantilever Functionally Graded Beam, *Journal of Reinforced Plastics and Composites*, 29(12), 1761-1774, 2010.
- Khosravi M., Jani M., Numerical resolution of large deflections in cantilever beams by Bernstein spectral method and a convolution quadrature. *International Journal of Nonlinear Analysis and Applications* 9(1), 117-127, 2018.
- Kimiaefar A., Domairry G., Mohebpour S.R., Sohoulı A.R., Davodi A.G., Analytical Solution for Large Deflections of a Cantilever Beam Under Nonconservative Load Based on Homotopy Analysis Method. *Numerical Methods for Partial Differential Equations* 27(3), 541-553, 2011.
- Kimiaefar A., Lund E., Thomsen O.T., Series solution for large deflections of a cantilever beam with variable flexural rigidity. *Meccanica* 47(7), 1787-1796, 2012.
- Kimiaefar A., Tolou N., Barari A., Herder, J.L., Large deflection analysis of cantilever beam under end point and distributed loads. *Journal of the Chinese Institute of Engineers* 37(4), 438-445, 2014.
- Li D.K., Li X.F., Large deflection and rotation of Timoshenko beams with frictional end supports under three-point bending. *Comptes Rendus Mecanique* 344(8), 556-568, 2019.
- Li S.R., Song X., Large thermal deflections of Timoshenko beams under transversely non-uniform temperature rise. *Mechanics Research Communications* 33(1), 84-92, 2006.
- Mien N.D., Gan B.S., Large deflections of tapered functionally graded beams subjected to end forces. *Applied Mathematical Modelling* 38(11-12), 3054-3066, 2014.
- Mohyeddin A., Fereidoon A., An analytical solution for the large deflection problem of Timoshenko beams under three-point bending. *International Journal of Mechanical Sciences* 78, 135-139, 2014.
- Rahimi G.H., Davoodinik A.R., Large Deflection of Functionally Graded Cantilever Flexible Beam with Geometric Non-Linearity: Analytical and Numerical Approaches. *Scientia Iranica Transaction B-Mechanical Engineering* 17(1), 25-40, 2010.
- Shen H.S., *Functionally Graded Materials Nonlinear Analysis of Plates and Shells*. CRC Press Taylor & Francis Group, Boca Raton, Florida, USA, 2009.
- Sitar M., Kosel F., Brojan M., Large deflections of nonlinearly elastic functionally graded composite beams. *Archives of Civil and Mechanical Engineering* 14(4), 700-709, 2014.
- Tari H., Kinzel G.L., Mendelsohn D.A., Cartesian and piecewise parametric large deflection solutions of tip point loaded Euler-Bernoulli cantilever beams. *International Journal of Mechanical Sciences* 100, 216-225, 2015.
- Ünal H., Ermiş K., Demirtaş Ş., Investigation of mechanical and microstructural properties of polyolefin rubber and glass beads filled polypropylene composites. *Journal of Materials and Mechatronics: A* 3(1), 91-105, 2022.
- Yin Y.Z., Wang Y.C., A numerical study of large deflection behaviour of restrained steel beams at elevated temperatures. *Journal of Constructional Steel Research* 60(7), 1029-1047, 2004.
- Zhou P., Liu Y., Liang X.Y., Analytical solutions for large deflections of functionally graded beams based on layer-graded beam model. *International Journal of Applied Mechanics* 10(9), DOI: 10.1142/S1758825118500989, 2018.